Ionics (2020) 26:1939–1950
https://doi.org/10.1007/s11581-019-03347-0

ORIGINAL PAPER

Allyl group-enabled side chain grafting for anion exchange membrane fabrication

Panyue Li[1] · Lei Bai[1] · Lingling Ma[1] · Naeem Akhtar Qaisrani[1] · Lv Li[1] · Yabin Jia[1] · Gaohong He[1] · Fengxiang Zhang[1]

Received: 10 August 2019 / Revised: 5 November 2019 / Accepted: 6 November 2019 / Published online: 4 December 2019

Abstract

In this paper, we report a novel type of anion exchange membrane, which was synthesized by polysulfone modification with N-methyl diallylamine, whose allyl group enabled subsequent graft copolymerization of 4-vinylbenzyl chloride (VBC) and styrene (ST); quaternization was achieved with N-methylmorpholine (Mm). By controlling the amount of VBC and ST, a series of grafted side chain-type anion exchange membranes, MmOH-PSf-VS-x (x standing for VBC content), was prepared. Attributed to good microphase separation, the MmOH-PSf-VS-12 membrane exhibited a high conductivity of 33.71 mS cm^{-1} at 20 °C, which is 34% higher than that of the N-methylmorpholine quaternized polysulfone membrane without side chains (MmOH-PSf) at a similar ion exchange capacity (IEC). Moreover, the swelling resistance and mechanical properties of the membranes were also improved with the side chain grafting. Our work provides a new route to fabricate side chain grafted anion exchange membrane (AEM).

Keywords N-methyl diallylamine · Microphase separation · Vinylbenzylchloride · Side chain · Anion exchange membrane

Introduction

Energy is especially important for the progress and development of human society. The main energy sources nowadays are fossil based, including petroleum, coal, and natural gas. However, the fossil fuels are limited and non-renewable, so it is necessary to develop alternatives to supplement and replace traditional fossil energies [1, 2]. Recently, fuel cells have been attracting intensive attention as a type of clean and efficient energy conversion technology; among them, proton exchange membrane fuel cells (PEMFCs) have been applied in laptop computers, bicycle, and mobile phones because of their high power density and low operating temperature, but the use of expensive platinum catalyst has become the main obstacle to their widespread application and commercialization [3–5]. In contrast, the alkaline anion exchange membrane fuel cell (AEMFC) shows enhanced redox reaction kinetics under the basic operating condition, and therefore does not rely on noble metals (Pt, Pd) as catalysts, which makes it a promising next generation energy technology [6–13].

As the core component of AEMFCs, the alkaline anion exchange membrane (AEM) separates the anode and cathode to avoid short circuit and meanwhile allows OH^- transport between them[14]. Currently, the main challenges of AEM development lie in its low conductivity and poor alkaline stability [15, 16]. To date, abundant efforts have been made to explore different cationic groups as the hydroxide ion exchange sites, including quaternary ammonium [17], guanidinium [18], phosphonium [19], piperidinium [20], morpholinium [21], imidazolium [22, 23], etc. Among these cation structures, piperidinium and pyrrolidinium are considered the most stable under alkaline condition [23–25], and for morpholinium, its oxygen atoms may build hydrogen bonds with water molecules, making the AEM more hydrophilic and more conductive [21, 26].

Apart from cation structure, the AEM property is also closely related to its ion exchange capacity (IEC) and the degree of microphase separation [27], the latter being able to provide pathways for ion transport. The main method to increase IEC is to increase graft density of cationic groups, but the AEM with high number of cationic groups directly tethered to the polymer backbone will suffer from backbone scission by prolonged hydroxide ion attack [28, 29]. So more and

✉ Fengxiang Zhang
zhangfx@dlut.edu.cn

[1] School of Chemical Engineering at Panjin, State Key Laboratory of Fine Chemicals, Dalian University of Technology, 2 Dagong Road, Panjin 124221, LN, China

more researchers tried to place the cation groups on side chains, making use of the difference between hydrophobic backbone and hydrophilic side chains to induce microphase separation and construct ion-conducting channels [11, 14, 27, 30, 31]. The microphase separated morphology of AEMs is typically achieved by designing multication side chain [11, 32–35] and comb-shaped [23, 31, 36] architectures. For instance, Hickner et al. reported side chain AEMs of multiple cations, where obvious hydrophilic–hydrophobic phase separation was observed from small angel X-ray scattering patterns and transmission electron microscopy images, and the membrane with three cations per side chain exhibited a high conductivity of 99 mS cm^{-1} at room temperature [35]. Xu et al. synthesized a comb-shaped AEM bearing locally and densely cation-functionalized side chains, which showed a microphase-separated morphology with nano-sized ionic clusters, and the resultant membrane exhibited high conductivity up to 0.1 S cm^{-1} at 80 °C [31].

Herein, we report the design and fabrication of a novel side chain-grafted AEM through an allyl route. The membrane was obtained by N-methyldiallyl amine modification of polysulfone and subsequent copolymerization of the allyl group with vinylbenzyl chloride (VBC) and styrene (ST); quaternization was achieved by the Menshutkin reaction between the chloromethyl group (from VBC) and N-methylmorpholine. This method is advantageous over the conventional VBC-based strategy, because the latter requires an ATRP (atom transfer radical polymerization) process which involves the use of catalyst and ligand. The addition of ST in the side chain grafting reaction is to tune the IEC of the membrane. By changing the feedings of VBC and ST proportionately, a series of side chain-grafted AEMs with different IECs were fabricated, which showed distinct hydrophilic–hydrophobic microphase separated morphology. Other properties, such as conductivity, stability, water uptake, etc. have also been studied.

Experimental details

General procedures and materials

Udel P-3500 Polysulfone (PSf) was supplied by Amoco Performance Products, Inc. Styrene (ST), 2,2′-Azobis(2-methylpropionitrile) (AIBN), N-methylmorpholine, vinylbenzylchloride (VBC), and N-methyldiallylamine were purchased from Aladdin Industrial Inc. Chloromethyl octyl ether (CMOE) was synthesized according to the literature [27]. All other chemicals such as N-methyl-2-pyrrolidolone (NMP, AR), sodium hydroxide (NaOH, AR), 1,2-dichloromethane (CH_2Cl_2, AR), dimethyl sulfoxide (DMSO, AR), and anhydrous tin chloride ($SnCl_4$) were commercially obtained and used as received.

Fabrication of the side chain grafted anion exchange membrane

PSf was chloromethylated following a literature method [27]. Next, 10-g chloromethylated PSf (or CMPSf) was dissolved in 150-mL NMP to make a solution, to which N-methyl diallylamine was added with the molar ratio of N-methyl diallylamine: CMPSf = 8:1. The mixture was stirred at 40 °C for 4 days and then precipitated in ethyl acetate. After repeated washing with ethyl acetate and filtering, the obtained solid (NPSf) was dried at room temperature for 48 h.

A total of 2-g NPSf was dissolved in 20-mL NMP in a 100-mL three-necked flask, and then VBC and ST were added (the molar ratio of NPSf: VBC: ST was 1:6:3 or 1:12:6). In order to remove water and oxygen in the reaction system, the flask was degassed and refilled with nitrogen gas for three times. Then AIBN was added to the reaction system quickly under the protection of nitrogen. After 24 h reaction at 65 °C, the mixture was cooled at room temperature and precipitated in ethyl acetate drop by drop. The resulting yellow solid was washed repeatedly and centrifuged for product collection. Finally, the product NPSf-VS-x (x = 6 or 12, representing the molar ratio VBC:NPSf) was dried at room temperature for 48 h.

The quaternization was implemented through NPSf-VS-x reacting with N-methyl- morpholine. Typically, 0.2-g NPSf-VS-x was dissolved in 4-mL DMSO, then N-methylmorpholine was added in slightly excess. The mixture was stirred at 80 °C for 24 h, and the resultant MmCl-PSf-VS-x solution was cast onto a clean glass plate with the size of 6 × 6 cm, then one dropper was used to make the solution spread evenly on the glass plate and dried at 60 °C for 24 h to obtain a uniform and transparent membrane. The MmCl-PSf-VS-x membranes were immersed in 1 M NaOH solution at room temperature for 24 h to obtain MmOH-PSf-VS-x membranes. Finally, all the membranes waiting test were stored in deionized water (DI) water in a sealed container. The thickness of the final membranes was 60 ± 5 μm.

Fabrication of the main chain type anion exchange membrane

The main chain type of anion exchange membrane (MmOH-PSf) was prepared as a control. The preparation is as follows: 0.15-g CMPSf was dissolved in 3-mL NMP, then N-methylmorpholine was added (the molar ratio of $-CH_2Cl$ to N-methylmorpholine is 1:3); after stirring at 80 °C for 24 h, the MmCl-PSf solution was centrifuged to remove insoluble impurities. Then the solution was cast onto a clean glass plate and dried at 60 °C for 24 h. The membrane obtained was treated 1 M NaOH solution at room temperature for 24 h. The subsequent treatments are the same as the MmOH-PSf-VS-x membranes.

Characterization and measurement

Spectroscopy

The polymers and membranes were characterized by ^{1}H NMR and Fourier transform infrared spectroscopy (FTIR). The ^{1}H NMR was implemented on a Bruker AVANCE III HD 500 spectrometer at a resonance frequency of 500 MHz; $CDCl_3$ or deuterated DMSO was used as the solvent and tetramethylsilane (TMS) as the internal standard. Fourier-transform infrared (FTIR) spectra were recorded on a Lambda-950 spectrometer with the wave number range of 500–4000 cm^{-1}.

Ionic exchange capacity (IEC)

The ion exchange capacity of the membrane was measured by back titration. The dry membrane with known weight was immersed in 20 mL 0.01 M HCl solution for 24 h at room temperature. Then 0.01 M NaOH solution was prepared and phenolphthalein was used as indicator to titrate residual HCl. The calculation of IEC follows the formula:

$$IEC = (C_{HCl}V_{HCl} - C_{NaOH}V_{NaOH})/W_{dry},$$

where C_{HCl} and C_{NaOH} are calibrated concentrations of HCl and NaOH respectively, while V_{HCl} and V_{NaOH} are the volume of HCl solution consumed before titration and the volume of NaOH solution consumed during back titration.

Water uptake and swelling ratio

The membrane waiting for testing was stored in degassed deionized water. The length (L_{wet}) of the wet sample was measured under the condition of full hydration and the weight (W_{wet}) was measured after wiping the water on the surface of the sample with absorbent paper. Then the sample was dried in a vacuum oven at 50 °C for 24 h; the weight (W_{dry}) and the length (L_{dry}) of the dry sample were measured again. Water uptake (WU) and swelling ratio (SR) were obtained by the following formulas:

$$WU = \left(W_{wet} - W_{dry}\right)/W_{dry}$$

$$SR = \left(L_{wet} - L_{dry}\right)/L_{dry},$$

respectively, where W_{wet} and W_{dry} represent the weight of the sample before and after drying, $Lwet = Lwet1 \times Lwet2^{1/2}$ and $L_{dry} = L_{dry1} \times L_{dry2}{}^{1/2}$ are the average length of the wet and dried samples, respectively; L_{wet1} and L_{wet2} are the length and width of wet sample, L_{dry1} and L_{dry2} are the length and width of dry sample, respectively.

Hydroxide conductivity

The conductivity test was carried out using traditional four-electrode electrochemical impedance spectroscopy (EIS) method on an Ivium-n-Stat N27133 electrochemical workstation with the frequency ranging from 10^5 Hz to 1 Hz. The membrane was cut into 4×1 cm^2 samples. During the test, the sample was placed between the upper and lower blocks of the testing mold, which was immersed in the deionized water. The conductivity (σ) is acquired by:

$$\sigma = L/(RA),$$

where L represents the distance (in cm) between two platinum wires in contact with the sample, R is the resistance (in Ohm) obtained from EIS curve, and A represents the surface area of the membrane sample.

Alkaline stability

The method to investigate alkaline stability is based on conductivity or IEC of the membranes after treatment in 1 M NaOH solution at 60 °C for different times. NaOH solution was refreshed every 2 days. The alkaline stability is assessed by comparing the conductivity or IEC before and after the alkaline treatment.

Thermal stability and mechanical properties

A Mettler Toledo thermogravimetric analyzer was used for thermogravimetric characterization. The temperature range is 30 ~ 800 °C with a heating rate of 10 °C/min and the heating ambience is N_2. The mechanical properties of the wet membrane were tested using a SANS electronic tensile tester in the air, and the tensile rate was 10 mm/min.

Morphology study

Morphology of the membranes were studied by using transmission electron microscopy (TEM) and small angel X-ray scattering (SAXS). For TEM, a dilute DMSO solution of the membrane sample was prepared, and a drop of the solution was applied onto the copper mesh, which was then dried at 60 °C for 24 h to remove the solvent and soaked in 1 M NaOH solution for 24 h to finish alkaline exchange. Then the copper mesh with membrane sample was washed with DI water for several times, soaked in a KI solution for 24 h, washed again with DI water to remove KI and dried in a vacuum oven at 50 °C for 24 h. Finally the sample was characterized using transmission electron microscopy.

The SAXS characterization was implemented to confirm the occurrence of microphase separation. The membrane sample (wet) was tested on D/Max-2400 powder X-ray scatterer.

The range of measurement angle was 0–5° and the rate was 1°/min. Scattering vector "*q*" and Bragg spacing "*d*" are calculated from the following formula: $q = 4\pi \sin\theta/\lambda$ and $d = 2\pi/q$, where 2θ represents the scattering angle and λ = 0.154 nm represents the scattering wavelength.

Results and discussion

Synthesis and structure characterization

The preparation of N-methylmorpholinium side chain grafted membrane (Mm-PSf-VS-x) is shown in Scheme 1. First, chloromethylated polysulfone (CMPSf) was functionalized with N-methyldiallylaminium, which then underwent free radical copolymerization with vinylbenzylchloride (VBC) and styrene (ST) via the allyl group. The resulting N-PSf was then quaternized with N-methylmorpholine to give MmCl-PSf-VS; finally, the membrane was treated with NaOH for alkalization.

The ^{1}H NMR spectra of CMPSf, N-PSf and N-PSf-VS-12 are shown in Fig. 1. The chemical shift at 4.46 ppm (Hc) corresponds to the $-CH_2Cl$ group, which confirms successful synthesis of CMPSf (Fig. 1a), whose degree of chloromethylation was 78% according to the peak area [22]. Figure 1b is the ^{1}H NMR spectrum of N-PSf. It can be clearly observed that there are chemical shifts at 5.58 ppm (H_{11}) and 6.09 ppm (H_{10}), which are the allyl proton signals of N-methyldiallylamine; the shifts at 2.89 ppm (H_8) and 3.88 ppm (H_9) correspond to the methyl and methylene groups on N-methyldiallylamine, respectively. All the above chemical shifts are assigned according to literature information [37], which proved the successful synthesis of N-PSf.

Figure 1c shows the ^{1}H NMR spectrum of the polymer N-PSf-VS-12. Compared with Fig. 1b, new signals appear at 1.17 ppm ($H_{10'}$, $H_{11'}$, and H_{12}), which correspond to methylene groups on the VBC-ST side chain [38–40]. The signals at 1.44 ppm (H_{13}) and 4.65 ppm (H_{16}) are assigned to protons of the methine on the side chain and $-CH_2Cl$ of VBC [31, 41–43], respectively. Characteristic signals corresponding to the allyl groups of N-PSf are still present at 6.07 ppm (H_{10}) and 5.58 ppm (H_{11}) because such groups were not fully reacted due to steric hindrance effect.

The N-PSf-VS-x polymer was quaternized by reacting with N-methylmorpholine. Figure 2 presents the ^{1}H NMR spectra of MmCl-PSf-VS-12 in comparison with MmCl-PSf, which does not have the side chains. In addition to those shown in Fig. 1, the signal at 3.07 ppm (Ha) corresponds to the methyl group of N-methylmorpholinium

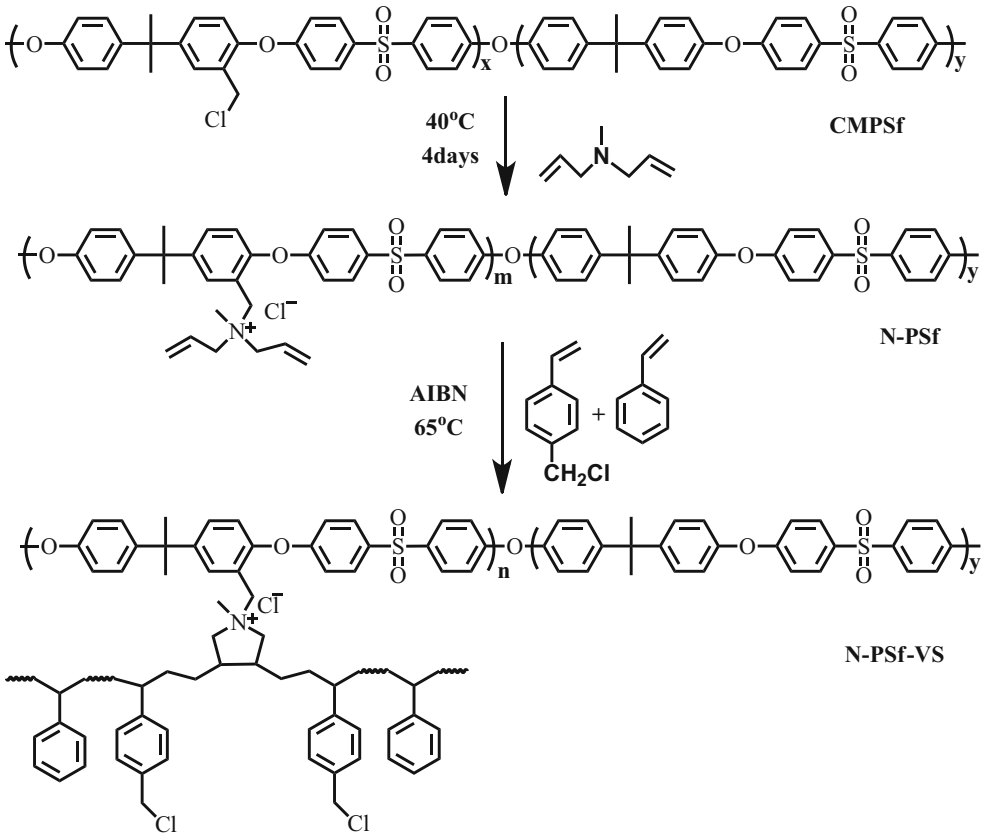

Scheme 1 Synthesis of the MmCl-PSf-VS

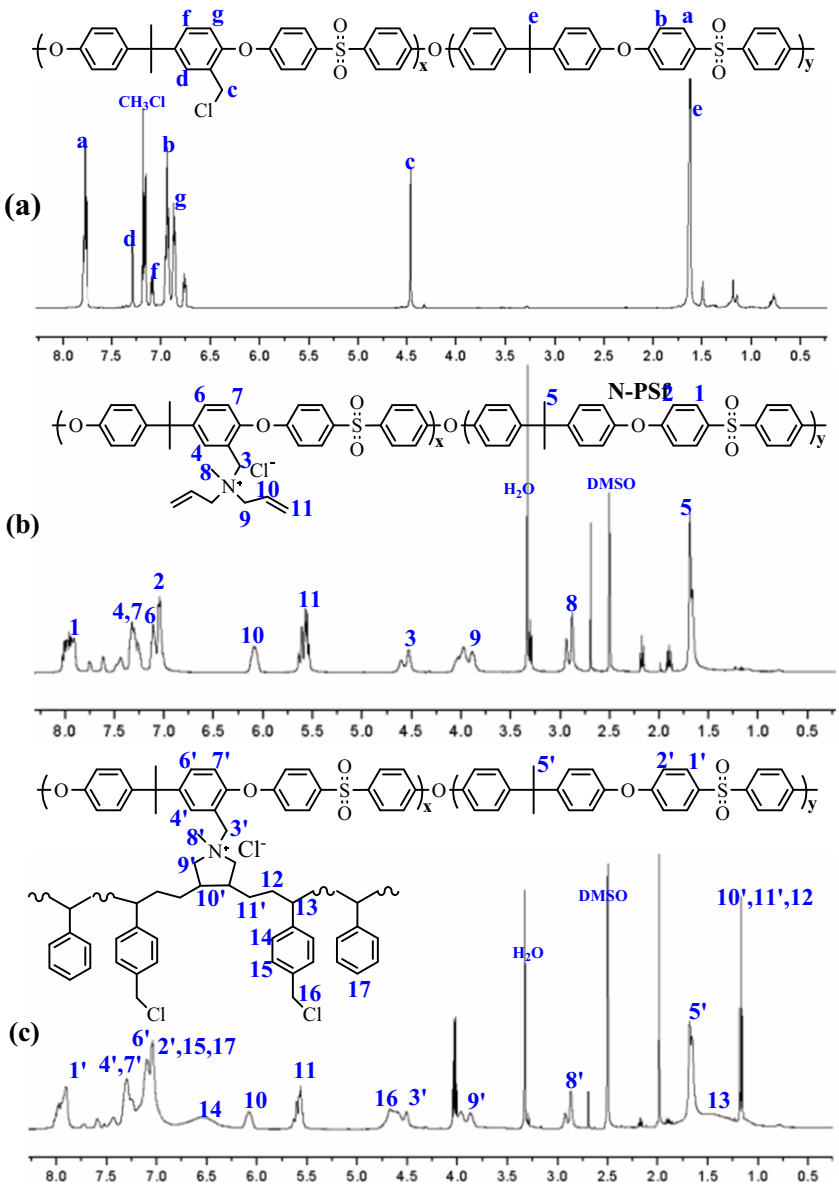

Fig. 1 ^{1}H NMR spectra of CMPSf **a**, N-PSf **b** and N-PSf-VS-12 **c**

(Fig. 2a); the signals at 3.54 ppm (Hc) and 2.33 ppm (Hb) correspond to the methylene close to O and N of N-methylmorpholine, respectively, which indicate the successful synthesis of MmCl-PSf-VS-12. Also in Fig. 2b, the signals at 3.51 ppm (H_3), 2.34 ppm (H_2) and 3.14 ppm (H_1) confirm the structure of MmCl-PSf synthesized as a control.

Water uptake (WU), swelling ratio (SR), and IEC

Water uptake, swelling ratio, and IEC are three closely related parameters which reflect the membrane performance. As is well known, the water molecules in the membrane can effectively promote the transport of OH^- via a vehicular mechanism, while excessive water will reduce the transport rate of OH^- due to a dilution effect, and the mechanical strength of the membrane will also be affected due to higher swelling ratio.

As seen from Table 1, the ungrafted NPSf membrane possesses a relatively low IEC (0.89 mmol g^{-1}), water uptake (31.87%), and swelling ratio (18.39%). When grafted with VBC and ST at a ratio of N-PSf:VBC:ST = 1:6:3, the resulting membrane (MmOH-PSf-VS-6) showed a significantly higher IEC of 1.55 mmol g^{-1} because the VBC-ST side chains provide multiple chloromethyl sites which can introduce more cationic groups as shown in Fig. 3. At the same time, the cationic groups caused higher water uptake (113%) and swelling ratio (29%) of the membrane. When increasing the feedings of VBC and ST (NPSf:VBC:ST = 1:12:6), the resultant membrane, MmOH-PSf-VS-12

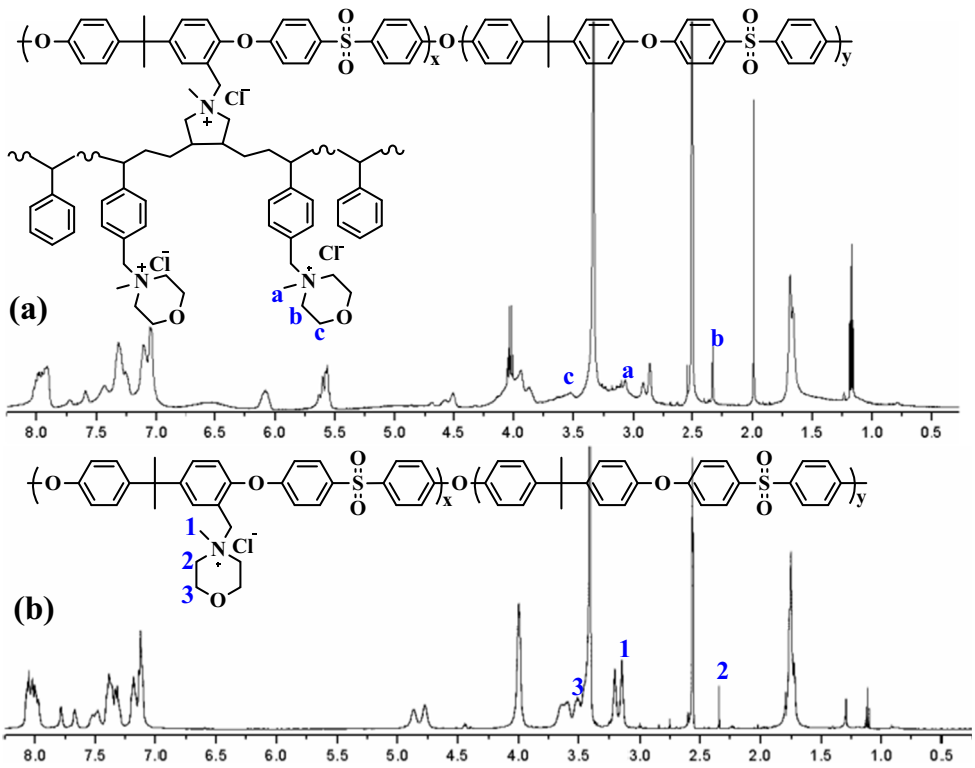

Fig. 2 ^{1}H NMR spectrum of MmCl-PSf-VS-12 **a** and MmCl-PSf **b**

showed a further increased IEC of 1.65 mmol g^{-1}, indicating that more VBC and ST were grafted to the side chain. Meanwhile, the water uptake and swelling ratio increase consistently with IEC.

It is noteworthy in Table 1 that the MmOH-PSf-VS-12 membrane exhibits lower water uptake (130% vs 182%) and lower swelling ratio (33% vs 57%) compared with the MmOH-PSf membrane which the cationic group is directly connected to the main chain at similar IEC, indicating that MmOH-PS-VS-12 membrane possesses better anti-swelling property. This is probably because the continuous hydrophobic domains formed by microphase separation, as will be seen in the subsequent section, can inhibit excessive water uptake of the membrane, and the lower grafting density of main chain is also beneficial to enhance the anti-swelling property of MmOH-PSf-VS-12. In addition, the un-quaternizable ST units in the VBC-ST side chain may play some role in inhibiting swelling.

Microphase separation

Microphase separation is very important for the anion exchange membrane. The separation of the hydrophilic–hydrophobic microphases can not only form larger hydrophilic channels for OH^{-} transport but also achieve better management of water molecules. The interconnected hydrophilic domains contribute to membrane conductivity, and continuous hydrophobic domains inhibit swelling of the membrane. In order to observe the microphase separation, the MmOH-PSf-VS-12, MmOH-PSf-VS-6, and MmOH-PSf membranes were characterized by transmission electron microscopy (TEM). Figure 4 shows the TEM micromorphology of different membranes, where the darker and brighter areas in the images correspond to hydrophilic domains and hydrophobic domains, respectively.

It is observed from Fig. 4a that in the TEM of MmOH-PSf membrane, small dark dots are scattered evenly throughout

Table 1 Water uptake, swelling ratio, and IEC at room temperature

Membrane	IEC(mmol g^{-1})	Water uptake(%)	Swelling ratio(%)
NPSf	0.89 ± 0.15	31.87 ± 0.50	18.39 ± 0.50
MmOH-PSf-VS-6	1.55 ± 0.19	113.22 ± 1.00	28.86 ± 0.88
MmOH-PSf-VS-12	1.65 ± 0.10	129.84 ± 1.23	32.87 ± 1.05
MmOH-PSf	1.63 ± 0.09	181.82 ± 1.90	57.08 ± 1.53

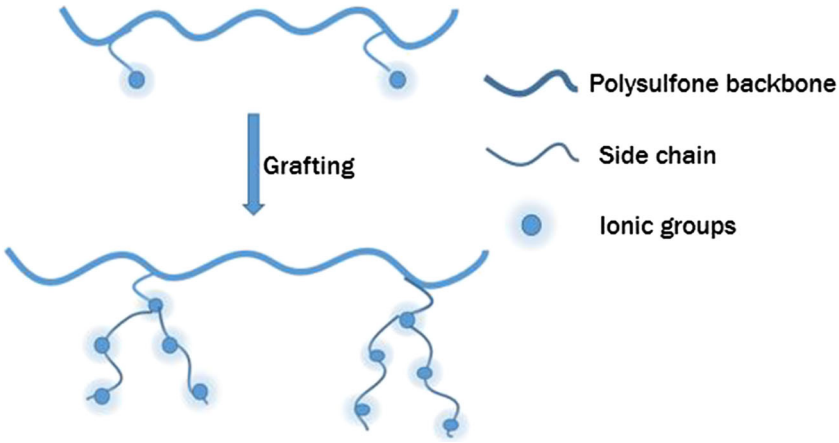

Fig. 3 Schema of pre-grafting and post-grafting

the whole area, which indicates that there is insignificant aggregation of cationic groups in the MmOH-PSf membrane, because the cationic groups directly connected to the main chain have lower mobility. When the main is grafted with VBC-ST side chains carrying cationic groups, the difference between hydrophobic backbone and hydrophilic side chain and higher mobility of side chain will induce distinct microphase separation. So compared with MmOH-PSf, the MmOH-PSf-VS-x membranes (Fig. 4b Fig. 4c) show larger hydrophilic domains, and form interconnected ion transport channels. In addition, the MmOH-PSf-VS-12 membrane (Fig. 4c) undergoes more distinct microphase separation than MmOH-PSf-VS-6 (Fig. 3b); this is because its longer flexible side chain increases cation mobility. This is also why the MmOH-PSf-VS-12 membrane and MmOH-PSf membrane have approximately the same IEC, but their micromorphology is very different, and forcedly highlights the superiority of the VBC-ST side chain grafted structure.

In order to further study the microphase separation in the membrane, the MmOH-PSf-VS-12 and MmOH-PSf membranes with similar IEC were characterized by small angle X-ray scattering (SAXS) spectroscopy. As can be seen from Fig. 5, no diffraction peak appears in the MmOH-PSf membrane while the MmOH-PSf-VS-12 membrane displays a sharp diffraction peak at $q = 0.68\ \mathrm{nm}^{-1}$, confirming the presence of distinct microphase separation, which is consistent with the observation from TEM. Based on the q value, the size of hydrophilic domains represented by the Bragg spacing d was estimated to be 9.24 nm according to the formula $d = 2\pi / q$; this size is bigger than that observed from TEM probably because the sample for SAXS measurement was wet, which may cause swelling of the ion cluster. Actually, the difference between TEM and SAXS obtained cluster sizes is sometimes reported in the literature.

Hydroxide conductivity

Conductivities of the MmOH-PSf-VS-x, MmOH–PSf, and ungrafted NPSf membranes at various temperatures are shown in Fig. 6. At room temperature, the ungrafted NPSf membrane

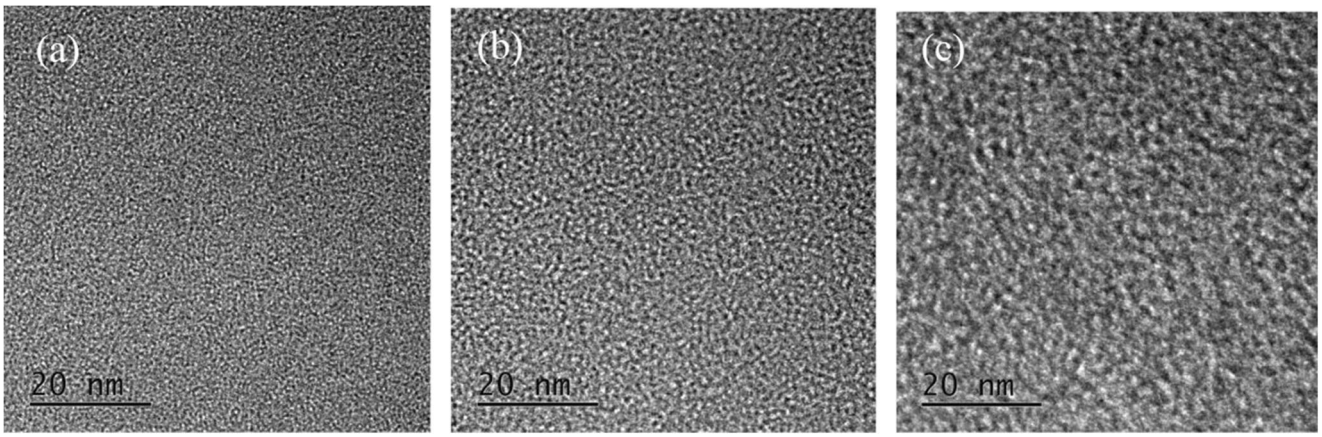

Fig. 4 TEM images of **a** MmOH-PSf (IEC = 1.63 mmol g^{-1}). **b** MmOH-PSf-VS-6 (IEC = 1.55 mmol g^{-1}). **c** MmOH-PSf-VS-12 (IEC = 1.65 mmol g^{-1}) membranes

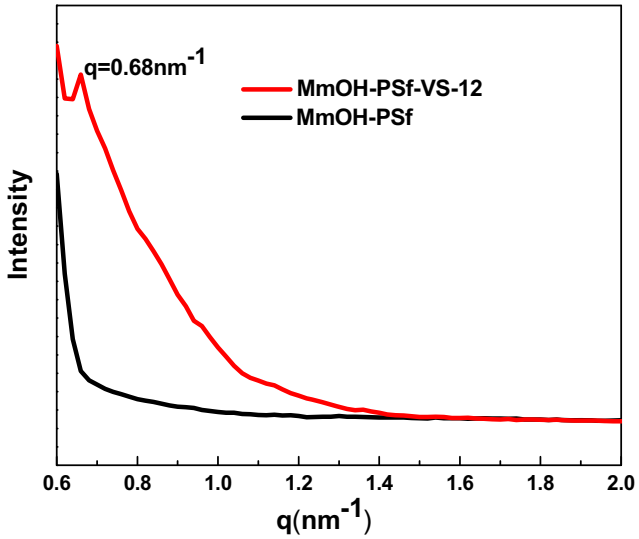

Fig. 5 SAXS graphs of MmOH-PSf-VS-12 and MmOH-PSf membranes

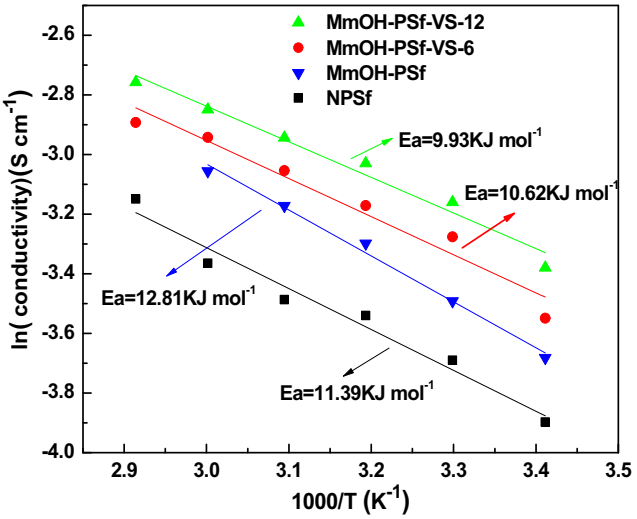

Fig. 7 Arrhenius plots of MmOH-PSf-VS-x, MmOH-PSf, and N-PSf membranes

showed a conductivity of 23.30 mS cm^{-1} (IEC = 0.89 mmol g^{-1}), while the MmOH-PSf-VS-6 and MmOH-PSf-VS-12 membranes showed 28.75 mS cm^{-1} (IEC = 1.55 mmol g^{-1}) and 33.71 mS cm^{-1} (IEC = 1.65 mmol g^{-1}), respectively, higher than that of NPSf due to the improvement of IEC and better microphase separated morphology, and the latter factor might be more important. The crucial role of microphase separation can be further manifested by the fact that the MmOH–PSf membrane with a high IEC of 1.63 mmol g^{-1} only shows a conductivity of 25.17 mS cm^{-1}, which is lower than that of MmOH-PSf-VS-12 (28.75 mS cm^{-1}) with a lower (IEC = 1.55 mmol g^{-1}). At elevated temperatures, all membranes show improved conductivities because of stronger mobility of ions and water molecules. At 70 °C, the MmOH-PSf-VS-12 membrane exhibited an excellent conductivity of 63.44 mS cm^{-1}, while the MmOH–PSf membrane was broken at 70 °C due to poor mechanical property because higher degree of functionalization weakens the Van Der Waals force among polymer chains, and the conductivity at 60 °C is 47.08 mS cm^{-1}.

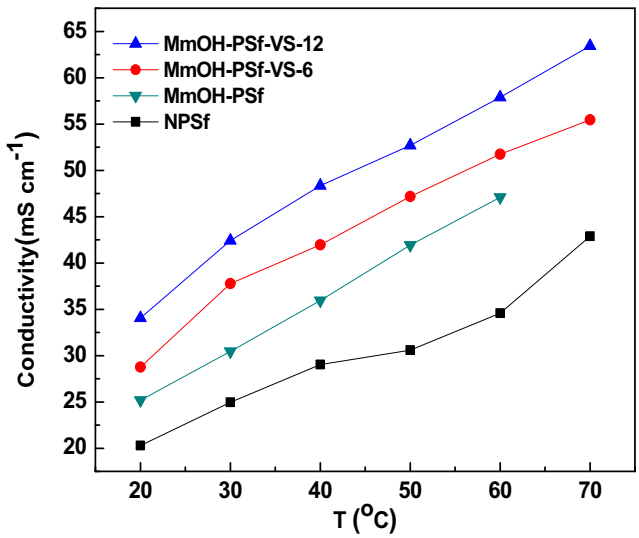

Fig. 6 Hydroxide conductivity of MmOH-PSf-VS and MmOH-PSf membranes as a function of temperature

In addition, the conductivity of prepared membranes obeys the Arrhenius behavior as shown in Fig. 7, where the activation energy of ion transport (E_a) was calculated. The larger the E_a is, more energy of ion transport is required. The value of E_a can be calculated by the formula $E_a = -bR$, where R represents the thermodynamic constant ($R = 8.314$ J $mol^{-1}K^{-1}$), and b is the slope of the ln(σ) 1000/T plot. As can be seen in Fig. 7, the MmOH-PSf-VS-12 membrane exhibits the smallest E_a while MmOH-PSf membrane the largest; that is why the former shows the highest and the latter shows the lowest conductivity, confirming the special VBC-ST grafted side chain can help construct smooth ion channels, reducing the resistance of ion transport in the AEM. It is worth noting from Table 2 that MmOH-PSf-VS-6 and -12 membranes are advantageous over some of the literature reported AEMs with comparable IEC in terms of conductivity. However, their water uptake and SR values are relatively high.

Alkaline stability

Alkaline stability of AEM is required to ensure reliability and long lifespan of anion exchange membrane fuel cell. Alkaline stability was assessed by immersing the membrane in 1 M NaOH solution at 60 °C, and monitoring its change in IEC and structure with time. As shown in Fig. 8a, the IEC of the MmOH-PSf-VS-6 and -12 membranes dropped with the immersion time, and ca. 80% and 79% of the original IEC value was retained, respectively, after the membrane was treated for

Table 2 Conductivity, WU, and SR properties of different membranes

Sample	IEC(mmol g^{-1})	WU(%)	SR(%)	Conductivity(mS cm^{-1})	Ref.
MmOH-PSF-VS-6	1.55	113.22	28.86	37.89 at 30 °C	This work
MmOH-PSF-VS-12	1.65	129.84	32.87	43.21 at 30 °C	This work
[PTMVPMA][OH]	1.62	92.56	22.35	15 at 30 °C	[44]
[PMVBIm][OH]	1.58	86.39	20.83	13 at 30 °C	[44]
$F_{30}C9N$	1.43	176	40	32 at 25 °C	[45]
PEN-MmOH	2.30	13.3	6.4	25 at 30 °C	[46]
BQA-FPAE-2	1.61	34.6	10.4	21.1 at 25 °C	[47]
QA-PS120-b-PDVPPA80-10C	1.67	17.9	5.1	25.5 at 20 °C	[48]

288 h; while the MmOH–PSf membrane at similar IEC was broken into pieces after the same treatment for just 48 h, meaning the grafted structure can alleviate alkali attack on the polymer backbone. However, as shown in Fig. 8b, the conductivity of the MmOH-PSf-VS-6 and -12 membranes gradually decreased with the time of immersion in the alkali solution. The inconsistent IEC and conductivity changes might be due to the possibility that the alkali-induced degradation of the morpholinium cation can produce tertiary amines (Fig. 9a); such products can react with HCl during the IEC measurement.

The MmOH-PSf-VS-6 membrane after treatment with 1 M NaOH solution at 60 °C for different periods were further characterized by FTIR. As shown in Fig. 9b, the bands at 1487 cm^{-1} and 1102 cm^{-1} corresponding to C-N^+ groups from the pyrodinium cation (formed by free radical polymerization of N-methyldiallylaminium with VBC and ST, see Scheme 1) did not show appreciable changes after the membrane was treated for 144 and 288 h, but the band at 1384 cm^{-1} became dwindled, indicating that some morpholinium cations have been degraded due to the hydroxide attack. Based on the above observations, our membrane right now is not stable enough compared with a lot of the literature reported ones, and needs further modification on the cation structure.

Thermal stability and mechanical properties

Figure 10 shows the thermogravimetric analysis (TGA) curves of MmOH-PSf-VS-12 and MmOH-PSf membranes. From the TGA, the weight losing process is mainly divided into three stages. The first stage mainly results from the volatilization of the bound water and residual solvent in the membrane, only 5% approximately. The onset decomposition temperature (T_{OD}) is a characteristic parameter to reflect the thermal decomposition process. The second weight losing stage is due to the degradation of cations of MmOH-PSf-VS-12 membrane (T_{OD} = 200 °C) and MmOH-PSf membrane (T_{OD} = 160 °C). This might be due to the better microphase separation in the MmOH-PSf-VS-12 membrane, where the resultant hydrophobic microphase can protect the cations against the thermal decomposition to some extent. The mass loss in the third stage corresponds to the degradation of polysulfone backbone (T_{OD} = 380 °C). Since the typical operating temperature of alkaline anion exchange membrane fuel cell (AAEMFCs)

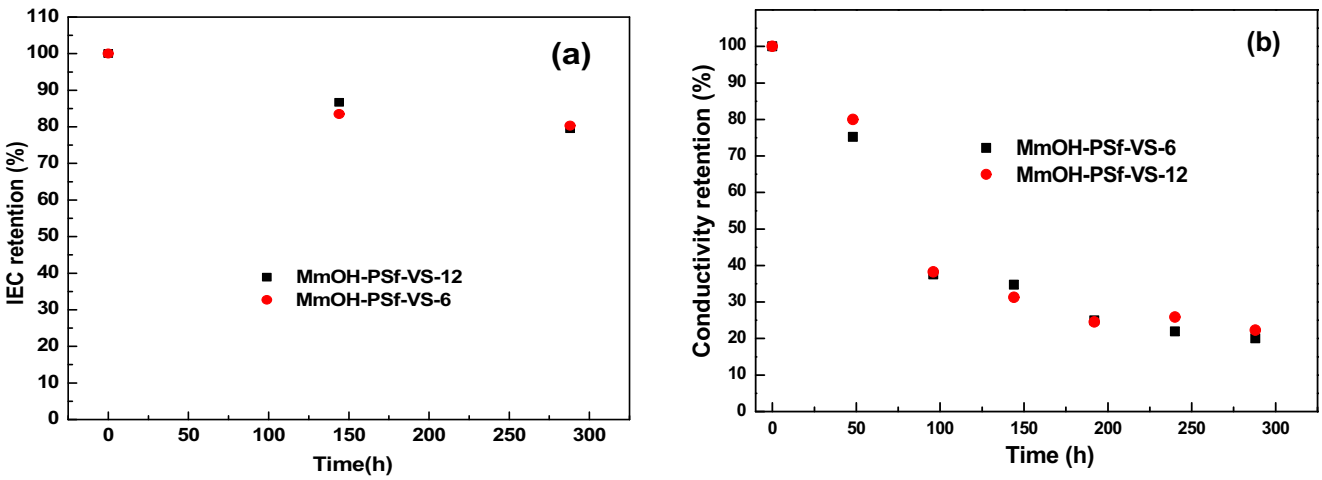

Fig. 8 The IEC (**a**) and conductivity (**b**) of MmOH-PSf-VS-6 and -12 membranes with increasing treatment time in 1 M NaOH at 60 °C. The conductivity was measured at 30 °C

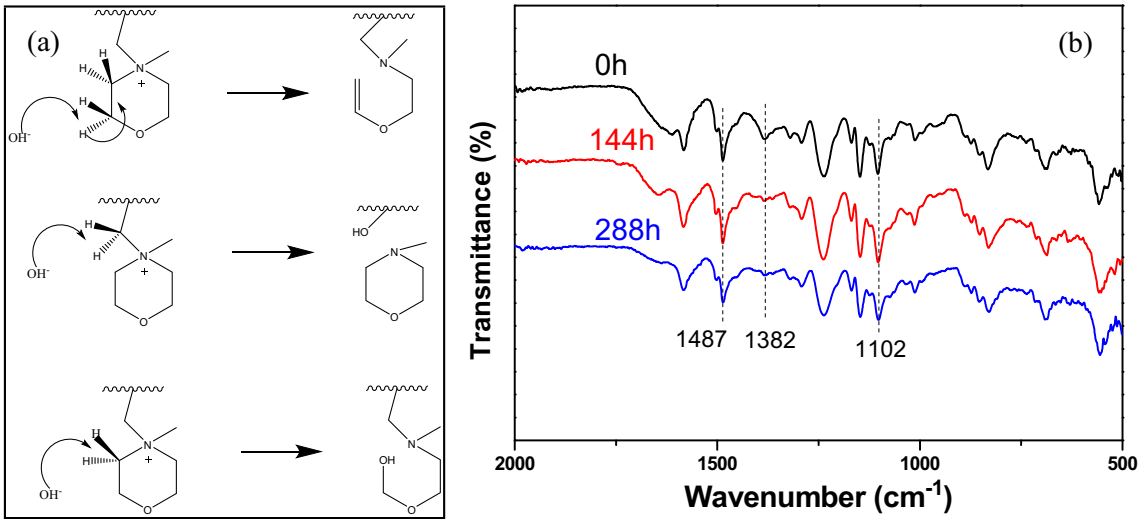

Fig. 9 **a** Possible pathways of morpholinium degradation. **b** FTIR spectra of the MmOH-PSf-VS-6 membrane treated in 1 M NaOH at 60 °C for different hours

ranges from 80 °C to 120 °C, the above thermal stability of the MmOH-PSf-VS-12 membrane can satisfy the requirement of fuel cell.

Table 3 shows the mechanical properties of the NPSf, MmOH-PSf-VS-x, and MmOH-PSf membranes at fully hydrated state. Compared with ungrafted NPSf membrane, the MmOH-PSf-VS-12 membrane has a higher IEC, but the mechanical strength was compromised due to higher water uptake and swelling ratio as shown in Table 1. When compared with MmOH-PSf at similar IEC, the MmOH-PSf-VS-12 membrane exhibits higher mechanical strength (4.37 MPa vs 2.36 MPa) and concomitantly lower elongation at break (9.84% vs 17.13%) because of its special VBC-ST grafted side chain structure, which has led to the formation of a well-developed microphase separated morphology as shown in Fig. 4 and Fig. 5, and consequently a strong framework that benefits the membrane strength.

After the alkali treatment in 1 M NaOH at 60 °C for 288 h, the MmOH-PSF-VS-6 membrane's tensile strength dropped from 4.78 to 2.39 MPa, and elongation at break dropped from 13.88 to 2.20%; the MmOH-PSF-VS-12 membrane also experienced a decay of mechanical properties, whose tensile strength decreased from 4.37 to 2.09 MPa and elongation at break from 9.84 to 9.29%, indicating a better backbone resistance to alkali attack because of higher grafting degree.

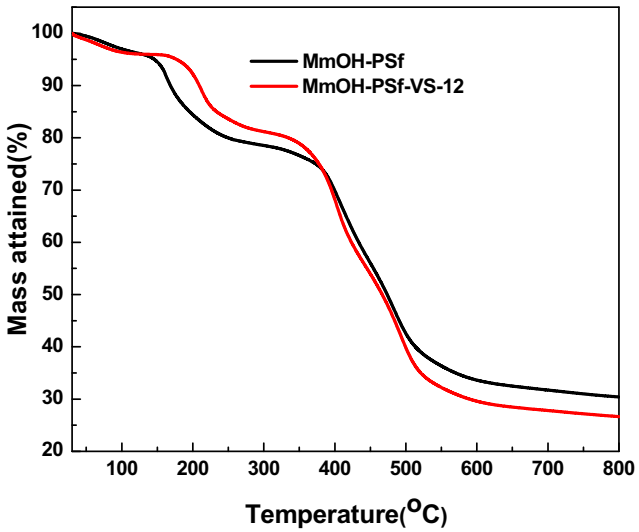

Fig. 10 TGA curves of MmOH-PSf-VS-12 and MmOH-PSf membranes

Conclusions

In summary, a novel VBC-ST grafted side chain anion exchange membrane was fabricated via polysulfone modification with N-methyl diallylamine and subsequent graft copolymerization of VBC and styrene ST with the allyl group, followed by a quaternization reaction between N-methylmorpholine and the chloromethyl group coming from VBC. By controlling the feeding amount of VBC and ST, side chain AEMs with different grafting degrees were obtained.

Table 3 Mechanical properties of N-PSf, MmOH-PSf-VS, and MmOH-PSf membranes in wet state

Membrane	IEC ($mmolg^{-1}$)	Tensile strength (MPa)	Elongation at break (%)
NPSf	0.89	12.03	20.06
MmOH-PSf-VS-6	1.55	4.78	13.88
MmOH-PSf-VS-12	1.65	4.37	9.84
MmOH-PSf	1.63	2.36	17.13

Compared with the main chain type MmOH-PSf membrane, the introduction of VBC-ST side chain greatly promotes the formation of microphase separated morphology, which was demonstrated by TEM and SAXS. Therefore, the MmOH-PSf-VS-12 membrane could obtain a higher conductivity of 33.71 mS cm^{-1} (20 °C) and 63.44 mS cm^{-1} (70 °C) than that of the ungrafted membrane. Meanwhile, the grafted membrane also showed a good alkali stability; ca. 80% of its IEC was retained after a 288-h alkali treatment in 1 M NaOH solution at 60 °C. Our work provides a new strategy of synthesizing side chain type AEM, which shows a good potential for application in fuel cells.

Funding information We acknowledge the financial supports from the National Natural Science Foundation of China (Grant no. 21776042), Science and Technology Innovation Fund of Dalian (2018J12GX052), the National Key Research and Development Program of China (Grant no. 2016YFB0101203), and China MOST (Ministry of Science and Technology) innovation team in key areas (No. 2016RA4053).

References

1. CHENG J, HE G, ZHANG F (2015) A mini-review on anion exchange membranes for fuel cell applications: stability issue and addressing strategies [J]. Int J Hydrog Energy 40(23):7348–7360
2. BOUDGHENE STAMBOULI A, Traversa E (2002) Fuel cells, an alternative to standard sources of energy[J]. Renew Sust Energ Rev 6(3):295–304
3. KIRUBAKARAN A, JAIN S, NEMA RK (2009) A review on fuel cell technologies and power electronic interface [J]. Renew Sust Energ Rev 13(9):2430–2440
4. ZHUO YZ, LAI AL, ZHANG QG et al (2015) Enhancement of hydroxide conductivity by grafting flexible pendant imidazolium groups into poly(arylene ether sulfone) as anion exchange membranes [J]. J Mater Chem A 3(35):18105–18114
5. AGEL E, BOUET J, FAUVARQUE JF (2001) Characterization and use of anionic membranes for alkaline fuel cells [J]. J Power Sources 101(2):267–274
6. ANTOLINI E, GONZALEZ ER (2010) Alkaline direct alcohol fuel cells [J]. J Power Sources 195(11):3431–3450
7. WANG X, Li M, Golding BT et al (2011) A polytetrafluoroethylene-quaternary 1,4-diazabicyclo-[2.2.2]-octane polysulfone composite membrane for alkaline anion exchange membrane fuel cells [J]. Int J Hydrog Energy 36(16): 10022–10026
8. YAN J, ZHU L, CHALOUX BL et al (2017) Anion exchange membranes by bromination of tetramethylbiphenol-based poly(sulfone)s [J]. Polym Chem 8(16):2442–2449
9. ZHU Y, HE Y, GE X et al (2018) A benzyltetramethylimidazolium-based membrane with exceptional alkaline stability in fuel cells: role of its structure in alkaline stability[J]. J Mater Chem A 6(2): 527–534
10. MANDAL M, HUANG G, KOHL PA (2019) Anionic multiblock copolymer membrane based on vinyl addition polymerization of norbornenes: applications in anion-exchange membrane fuel cells[J]. J Membr Sci 570-571:394–402
11. LIU L, CHU X, LIAO J et al (2018) Tuning the properties of poly(2,6-dimethyl-1,4-phenylene oxide) anion exchange membranes and their performance in H2/O2 fuel cells[J]. Energy Environ Sci 11(2):435–446
12. YANG C, LIU L, HAN X et al (2017) Highly anion conductive, alkyl-chain-grafted copolymers as anion exchange membranes for operable alkaline H2/O2 fuel cells[J]. J Mater Chem A 5(21): 10301–10310
13. RAN J, WU L, RU Y et al (2015) Anion exchange membranes (AEMs) based on poly(2,6-dimethyl-1,4-phenylene oxide) (PPO) and its derivatives[J]. Polym Chem 6(32):5809–5826
14. LIN CX, HUANG XL, GUO D et al (2016) Side-chain-type anion exchange membranes bearing pendant quaternary ammonium groups via flexible spacers for fuel cells[J]. J Mater Chem A 4(36):13938–13948
15. TANAKA M, FUKASAWA K, NISHINO E et al (2011) Anion conductive block poly(arylene ether)s: synthesis, properties, and application in alkaline fuel cells[J]. J Am Chem Soc 133(27): 10646–10654
16. PAN ZF, AN L, ZHAO TS et al (2018) Advances and challenges in alkaline anion exchange membrane fuel cells[J]. Prog Energy Combust Sci 66:141–175
17. PAN J, LU S, LI Y et al (2010) High-performance alkaline polymer electrolyte for fuel cell applications[J]. Adv Funct Mater 20(2): 312–319
18. WANG J, LI S, ZHANG S (2010) Novel hydroxide-conducting polyelectrolyte composed of an poly(arylene ether sulfone) containing pendant quaternary guanidinium groups for alkaline fuel cell applications[J]. Macromolecules 43(8):3890–3896
19. TANG H, LI D, Li N et al (2018) Anion conductive poly(2,6-dimethyl phenylene oxide)s with clicked bulky quaternary phosphonium groups[J]. J Membr Sci 558:9–16
20. KIM S, YANG S, KIM D (2017) Poly(arylene ether ketone) with pendant pyridinium groups for alkaline fuel cell membranes[J]. Int J Hydrog Energy 42(17):12496–12506
21. LIU J, YAN X, GAO L et al (2019) Long-branched and densely functionalized anion exchange membranes for fuel cells[J]. J Membr Sci 581:82–92
22. ZHANG F, ZHANG H, QU C. (2011) Imidazolium functionalized polysulfone anion exchange membrane for fuel cell application[J]. J Mater Chem 21(34):12744
23. PONCE-GONZ LEZ J, WHELLIGAN DK, WANG L et al (2016) High performance aliphatic-heterocyclic benzyl-quaternary ammonium radiation-grafted anion-exchange membranes[J]. Energy Environ Sci 9(12):3724–3735
24. OLSSON JS, PHAM TH, JANNASCH P (2018) Poly(arylene piperidinium) Hydroxide ion exchange membranes: synthesis, alkaline stability, and conductivity [J]. Advanced Functional Materials 28(2):1702758
25. GU F, DONG H, LI Y et al (2014) Base stable pyrrolidinium cations for alkaline anion exchange membrane applications[J]. Macromolecules 47(19):6740–6747
26. GONG F, WANG R, CHEN X et al (2017) Facile synthesis and the properties of novel cardo poly(arylene ether sulfone)s with pendent cycloaminium side chains as anion exchange membranes[J]. Polym Chem 8(29):4207–4219
27. PAN Y, ZHANG Q, YAN X et al (2018) Hydrophilic side chain assisting continuous ion-conducting channels for anion exchange membranes[J]. J Membr Sci 552:286–294
28. XIAO LIN C, QIN WANG X, NING HU E et al (2017) Quaternized triblock polymer anion exchange membranes with enhanced alkaline stability[J]. J Membr Sci 541:358–366
29. LI Q, LIU L, MIAO Q et al (2014) A novel poly(2,6-dimethyl-1,4-phenylene oxide) with trifunctional ammonium moieties for alkaline anion exchange membranes[J]. Chem Commun 50(21):2791–2793
30. HOU J, WANG X, LIU Y et al (2016) Wittig reaction constructed an alkaline stable anion exchange membrane[J]. J Membr Sci 518: 282–288

31. RAN J, WU L, XU T (2013) Enhancement of hydroxide conduction by self-assembly in anion conductive comb-shaped copolymers[J]. Polym Chem 4(17):4612
32. LI L, LIN CX, WANG XQ et al (2018) Highly conductive anion exchange membranes with long flexible multication spacer[J]. J Membr Sci 553:209–217
33. LIN CX, WU HY, LI L et al (2018) Anion conductive triblock copolymer membranes with flexible multication side chain[J]. ACS Appl Mater Interfaces 10(21):18327–18337
34. HU C, ZHANG Q, LIN C et al (2018) Multi-cation crosslinked anion exchange membranes from microporous Tröger's base copolymers[J]. J Mater Chem A 6(27):13302–13311
35. ZHU L, PAN J, WANG Y et al (2016) Multication side chain anion exchange membranes[J]. Macromolecules 49(3):815–824
36. WANG L, MAGLIOCCA E, CUNNINGHAM EL et al (2017) An optimised synthesis of high performance radiation-grafted anion-exchange membranes[J]. Green Chem 19(3):831–843
37. OLSSON JS, PHAM TH, JANNASCH P (2017) Poly(N,N-diallylazacycloalkane)s for anion-exchange membranes functionalized with N-spirocyclic quaternary ammonium cations[J]. Macromolecules 50(7):2784–2793
38. HAO J, GAO X, JIANG Y et al (2018) Crosslinked high-performance anion exchange membranes based on poly(styrene-b -(ethylene- co -butylene)- b -styrene)[J]. J Membr Sci 551:66–75
39. WANG Z, LI Z, CHEN N et al (2018) Crosslinked poly (2,6-dimethyl-1,4-phenylene oxide) polyelectrolyte enhanced with poly (styrene-b-(ethylene-co-butylene)-b-styrene) for anion exchange membrane applications[J]. J Membr Sci 564:492–500
40. ZHAO Y, YU H, YANG D et al (2013) High-performance alkaline fuel cells using crosslinked composite anion exchange membrane[J]. J Power Sources 221:247–251
41. OHASHI H, JUNG H, CHI X et al (2018) Alkali-resistant anion exchange membranes with grafted polyelectrolyte for fuel cells[J]. Chem Lett 47(7):857–859
42. GE Q, LIANG X, DING L et al (2019) Guiding the self-assembly of hyperbranched anion exchange membranes utilized in alkaline fuel cells[J]. J Membr Sci 573:595–601
43. LI S, GAN R, LI L et al (2017) Highly branched side chain grafting for enhanced conductivity and robustness of anion exchange membranes[J]. Ionics 24(1):189–199
44. QIU B, LIN B, QIU L et al (2012) Alkaline imidazolium- and quaternary ammonium-functionalized anion exchange membranes for alkaline fuel cell applications[J]. J Mater Chem 22(3):1040–1045
45. ZHU L, PENG X, SHANG SL et al (2019) High performance anion exchange membrane fuel cells enabled by fluoropoly(olefin) membranes[J]. Adv Funct Mater 1902059
46. YAN X, DENG R, PAN Y et al (2017) Improvement of alkaline stability for hydroxide exchange membranes by the interactions between strongly polar nitrile groups and functional cations[J]. J Membr Sci 533:121–129
47. ZHANG J, HE Y, LIANG X et al (2019) Towards the gemini cation anion exchange membranes by nucleophilic substitution reaction. [J]. Science China Materials
48. ZHU M, ZHANG X, SU Y et al (2019) Comb-shaped diblock copolystyrene for anion exchange membranes [J]. J Appl Polym Sci 136(15):47370